Error Analysis of Finite-Element Solutions for Postbuckled Plates

Rajaram Sistla* and Gaylen A. Thurston†
NASA Langley Research Center, Hampton, Virginia

This paper is a continuation of a previous paper on the error analysis of results from finite-element solutions of problems in shell structures. The previous paper outlined a general approach based on the observation that many structures are an assembly of individual shell components. Therefore, for each component shell, results for stresses and deflections from finite-element solutions should agree with the corresponding results from shell theory. The general approach was applied to stiffened panels that contain orthotropic, postbuckled, rectangular plate components. The analytical results from plate theory were satisfactory except for an oscillatory behavior on the boundary between nodal points of the finite-element solution. This paper presents the results of additional numerical analysis that eliminates the oscillatory behavior. Also, the theory is extended to include plates with initial geometric imperfections. The new analysis has been programmed as a postprocessor for a general-purpose finite-element code. Numerical results are presented for a stiffened panel in compression and for a plate loaded in shear by a picture-frame test fixture.

Nomenclature

$A_{11},A_{12},A_{22},A_{66}$	= extensional stiffnesses of orthotropic plate
A_{mn},N_{3mn}	= Fourier sine-sine series coefficients
a,b	= dimensions of rectangular plate
$D_{11},D_{12},D_{22},D_{66}$	= bending stiffnesses of orthotropic plate
E	= residual error
f,g	= dummy variables in linear operators
$L_{ij}(\ )\ i=1,2;\ j=1,2$	= linear operators
M_x,M_y,M_{xy}	= moment stress resultants
N_x,N_y,N_{xy}	= in-plane stress resultants
$N_i(\ ,\ )\ i=1,3$	= nonlinear operators
Q_x,Q_y	= transverse shear stress resultants
U,V,W	= plate displacements
U_E,U_I	= series solutions for U
V_E,V_I	= series solutions for V
W_E,W_I	= series solutions for W
$\bar{W}$	= initial out-of-plane imperfection
x,y	= Cartesian coordinates
$\beta=a/b$	= plate aspect ratio
$\epsilon_x,\epsilon_y,\epsilon_{xy}$	= in-plane strains
$\xi=2\pi x/a,\ \eta=2\pi y/b$	= dimensionless coordinates

Subscripts

x and y following a comma denote partial derivative of principal symbol with respect to the subscript.

Presented as Paper 88-2216 at the AIAA/ASME/ASCE/AHS 29th Structures, Structural Dynamics and Materials Conference, Williamsburg, VA, April 18-20, 1988; received May 20, 1988; revision received Oct. 24, 1988.

*Research Engineer, Analytical Services and Materials, Inc. Senior Member AIAA.

†Senior Aerospace Engineer, Structural Mechanics Branch, Structural Mechanics Division. Associate Fellow AIAA.

Introduction

ESTIMATING the accuracy of stresses and deflections computed by the finite-element method is a common problem that arises with each new application of the method. Research on error analysis is reported in an earlier paper.[1] That paper outlines a general approach to error analysis using Newton's method for solving the Euler equations of shell theory for components of shell structures with continuous geometry, loads, and material properties and using substructuring to satisfy the continuity conditions for stresses and deformations between shell components. In this approach, the finite-element results become a zeroth approximation in Newton's method.

The general approach[1] was applied to discrete results for postbuckled plate components from a general-purpose finite-element code to compute a continuous approximation for the solution of the plate equations. To generate the continuous solution, a collocation method was used to match the finite-element displacements at nodal points on the plate boundary. The continuous solution exhibited oscillatory behavior between nodal points on the boundary while giving a satisfactory measure of error at interior points.

The current paper is concerned with two extensions of the previous results for error analysis of postbuckled plate components. First, the oscillatory behavior of the continuous solutions on the plate boundary has been reduced by satisfying the boundary conditions using the least-squares method. Second, error analysis has been extended to include plates with initial geometric imperfections.

The numerical analysis for satisfying boundary conditions by a least-squares method is outlined and contour plots of results for a sample problem are presented. The plots compare results from a finite-element code,[2] continuous solutions using collocation[1] for matching boundary conditions, and the new continuous solutions based on the least-squares method. The continuous solutions based on the least-squares method are smoother than the previous results from collocation, and they allow computation of deflections and stress resultants at any coordinate point on the plate. An exact expression for the residual error in the equilibrium equation in the direction normal to the plane of the plate is also evaluated. This residual error is a measure of the accuracy of the continuous solution, and is a result that is not duplicated by any finite-element

codes that are based on direct minimization of a variational principle.

The error analysis for plates with initial imperfections in shape is outlined in this paper. Results from a general-purpose finite-element code[2] are compared with the continuous solution for a postbuckled, imperfect, graphite-epoxy plate under in-plane shear loads. The imperfection shape and plate properties are those of a plate tested and analyzed by Rouse.[3]

Theory for Imperfect Plates

A well-posed problem for a postbuckled plate component requires a set of plate equations plus a set of boundary conditions. This section lists the equations for an orthotropic, imperfect plate and outlines a method for deriving a continuous solution in generalized coordinates from a set of discrete finite-element results. Some of the generalized coordinates are constants of integration that are determined by the boundary conditions. The analysis reported here uses the nodal displacements in the finite-element results as a first approximation for boundary conditions. The numerical analysis for a least-squares fit of the discrete boundary conditions is outlined in this section, and more details are contained in the Appendix.

Once the numerical values of constants of integration are determined, the continuous solution in generalized coordinates is completely defined for the plate component, and continuous results are determined for comparison with the corresponding discrete results. Stress resultants and deflections can be computed at any point on the plate, not merely at grid points of the discrete solution. Finally, a residual error is computed from the continuous solution by direct substitution in the nonlinear equilibrium equation in the direction of the normal to the plate reference surface.

Constitutive Relations

The theory applies to orthotropic plates with the following constitutive relations:

$$N_x = A_{11}\epsilon_x + A_{12}\epsilon_y \tag{1a}$$

$$N_y = A_{12}\epsilon_x + A_{22}\epsilon_y \tag{1b}$$

$$N_{xy} = A_{66}\epsilon_{xy} \tag{1c}$$

$$M_x = D_{11}W_{,xx} + D_{12}W_{,yy} \tag{2a}$$

$$M_y = D_{12}W_{,xx} + D_{22}W_{,yy} \tag{2b}$$

$$M_{xy} = 2D_{66}W_{,xy} \tag{2c}$$

where the strain-displacement relations for the imperfect plate are

$$\epsilon_x = U_{,x} + \tfrac{1}{2}W_{,x}^2 + W_{,x}\bar{W}_{,x} \tag{3a}$$

$$\epsilon_y = V_{,y} + \tfrac{1}{2}W_{,y}^2 + W_{,y}\bar{W}_{,y} \tag{3b}$$

$$\epsilon_{xy} = U_{,y} + V_{,x} + W_{,x}W_{,y} + W_{,x}\bar{W}_{,y} + W_{,y}\bar{W}_{,x} \tag{3c}$$

Equilibrium Equations

The equations that determine the transverse shear stress resultants are moment equilibrium equations:

$$Q_x = M_{x,x} + M_{xy,y} \tag{4a}$$

$$Q_y = M_{y,y} + M_{xy,x} \tag{4b}$$

The in-plane equilibrium equations are

$$N_{x,x} + N_{xy,y} = 0 \tag{5a}$$

$$N_{xy,x} + N_{y,y} = 0 \tag{5b}$$

The transverse force equilibrium equation is

$$Q_{x,x} + Q_{y,y} - N_3(F, W + \bar{W}) = 0 \tag{5c}$$

Where the notation $N_3(F, W + \bar{W})$ is a shorthand notation for

$$N_3(F, W + \bar{W}) = N_3(F, W) + N_3(F, \bar{W}) \tag{6a}$$

$$N_3(F, W) = N_x W_{,xx} + 2N_{xy}W_{,xy} + N_y W_{,yy} \tag{6b}$$

Displacement Equations and Boundary Conditions

The constitutive relations, strain-displacement relations, and moment equilibrium equations are substituted to reduce the three force equilibrium equations, Eq. (5), to three partial differential equations in the three displacement components U, V, and W:

$$L_{11}(U) + L_{12}(V) + N_1(W, W) + N_1(W, \bar{W}) + N_1(\bar{W}, W) = 0 \tag{7a}$$

$$L_{12}(U) + L_{22}(V) + N_2(W, W) + N_2(W, \bar{W}) + N_2(\bar{W}, W) = 0 \tag{7b}$$

$$L_{33}(W) - N_3(F, W) - N_3(F, \bar{W}) = 0 \tag{7c}$$

where

$$L_{11}(U) = A_{11}U_{,xx} + A_{66}U_{,yy} \tag{8a}$$

$$L_{12}(f) = (A_{12} + A_{66})f_{,xy} \tag{8b}$$

$$L_{22}(V) = A_{22}V_{,yy} + A_{66}V_{,xx} \tag{8c}$$

$$L_{33}(W) = D_{11}W_{,xxxx} + 2(D_{12} + 2D_{66})W_{,xxyy} + D_{22}W_{,yyyy} \tag{8d}$$

$$N_1(f,g) = A_{11}f_{,x}g_{,xx} + (A_{12} + A_{66})f_{,y}g_{,xy} + A_{66}f_{,x}g_{,yy} \tag{8e}$$

$$N_2(f,g) = A_{22}f_{,y}g_{,yy} + (A_{12} + A_{66})f_{,x}g_{,xy} + A_{66}f_{,y}g_{,xx} \tag{8f}$$

Continuous Solution for W

The continuous solution for W consists of two series solutions W_E and W_I.

$$W = W_I + W_E \tag{9a}$$

The generalized coordinates in each series are computed from discrete[2] data; W_I from data at centroids of elements and W_E from data on the plate boundary. The functions W_I and W_E are defined to satisfy two partial differential equations

$$L_{33}(W_I) = N_3(F_0, W_0) + N_3(F_0, \bar{W}) \tag{9b}$$

$$L_{33}(W_E) = 0 \tag{9c}$$

The numerical results for continuous solutions in this paper are for rectangular plate components that are modeled with rectangular elements defined by a rectangular grid of node points. The zero subscript on the right-hand side of Eq. (9b) denotes discrete[2] data that are computed and stored only at the centroids of the rectangular elements. The continuous solution for W_I is computed by first using numerical harmonic analysis[4] to compute the coefficients N_{3mn} in a double Fourier sine series

$$N_3(F_0, W_0 + \bar{W}) = \sum_{m=1}^{M-1}\sum_{n=1}^{N-1} N_{3mn} \sin\frac{m\pi x}{a} \sin\frac{n\pi y}{b} \tag{10a}$$

The Fourier series on the right-hand side of Eq. (10a) passes through the tabulated values of the left-hand side. The tabulated values are at centroids of the elements in the finite-element (FEM) model. The number of terms in the series is deter-

mined by M and N, the number of rows and columns in the FEM model. The generalized coordinates in the continuous solution W_I are the Fourier coefficients A_{mn} in the series

$$W_I = \sum_{m=1}^{M-1} \sum_{n=1}^{N-1} A_{mn} \sin\frac{m\pi x}{a} \sin\frac{n\pi y}{b} \tag{10b}$$

Substituting Eqs. (10) into Eq. (9b) determines the numerical values of the A_{mn}.

$$A_{mn} = \frac{a^4}{\pi^4} \frac{N_{3mn}}{[D_{11}m^4 + 2(D_{12} + 2D_{66})m^2n^2\beta^2 + D_{22}n^4\beta^4]} \tag{10c}$$

In general, the continuous solution W_I does not satisfy the plate boundary and/or continuity conditions. The solution W_E is added to W_I to obtain a better fit of the discrete results on the boundary. The solution W_E is assumed as a series that satisfies Eq. (9c) term by term.

$$W_E = W_{00} + \sum_{p=1} [W_{pc}(\eta) \cos p\xi + W_{ps}(\eta) \sin p\xi] + \sum_{q=1} [W_{qc}(\xi) \cos q\eta + W_{qs}(\xi) \sin q\eta] \tag{11}$$

The first term is a polynomial with undetermined coefficients

$$W_{00} = a_{00} + a_{10}x + a_{01}y + a_{20}x^2 + a_{02}y^2 \tag{12}$$

Each of the functions $W_{pc}(\eta)$, $W_{ps}(\eta)$, $W_{qc}(\xi)$, and $W_{qs}(\xi)$ satisfies a fourth-order, homogeneous, ordinary differential equation[1] and, consequently, contains four constants of integration that make up the set of generalized coordinates for W_E.

Boundary Conditions for W

The undetermined coefficients in W_{00} and the constants of integration in the functions $W_{pc}(\eta)$, $W_{ps}(\eta)$, $W_{qc}(\xi)$, and $W_{qs}(\xi)$ are computed from FEM output on the plate boundary. The output at nodal points for W and $W_{,x}$ on sides with constant x and for W and $W_{,y}$ on sides with constant y becomes the discrete boundary conditions for the continuous solution for W.

The constants of integration in the product solutions in W_E are computed by a least-squares analysis of the equations

$$W_E = W_0 - W_I \quad \text{for } x = 0 \tag{13a}$$

$$W_E = W_0 - W_I \quad \text{for } x = a \tag{13b}$$

$$W_{E,x} = W_{0,x} - W_{I,x} \quad \text{for } x = 0 \tag{13c}$$

$$W_{E,x} = W_{0,x} - W_{I,x} \quad \text{for } x = a \tag{13d}$$

$$W_E = W_0 - W_I \quad \text{for } y = 0 \tag{14a}$$

$$W_E = W_0 - W_I \quad \text{for } y = b \tag{14b}$$

$$W_{E,y} = W_{0,y} - W_{I,y} \quad \text{for } y = 0 \tag{14c}$$

$$W_{E,y} = W_{0,y} - W_{I,y} \quad \text{for } y = b \tag{14d}$$

For example, four equations containing the four constants of integration appearing in the function $W_{rc}(\eta)$, where r is an integer, are generated from Eqs. (13) by multiplying the displacement conditions by $\cos r\eta$ and the slope conditions by $\sin r\eta$ and integrating from 0 to 2π. Terms in $W_{qc}(\eta)$ for $q \neq r$ drop out of the four integrals along with all of the functions $W_{qs}(\eta)$. However, the integrals determine small nonzero coefficients multiplying the constants of integration appearing in the functions $W_{pc}(\eta)$ and $W_{ps}(\eta)$.

In a corresponding fashion, four integrals are written for each trigonometric function $\sin q\eta$, $\cos p\xi$, and $\sin p\xi$ appearing in W_E. Integrals are also written containing nonzero multipliers of the undetermined coefficients in W_{00}. Four of these latter integrals are integrals of Eqs. (13c), (13d), (14c), and (14d). An additional equation containing the coefficient a_{00} is derived by summing the four integrals of Eqs. (13a), (13b), (14a), and (14b). These integrals are connected with smoothing the numerical results on the boundary. They replace integrals used in the numerical computations in Ref. 1 and are listed in the Appendix.

The integrals derived from the left-hand sides of Eqs. (13) and (14) are equated to corresponding integrals of the right-hand sides. Since the notation W_0 refers to FEM data at nodal points on the plate boundary, the integrals containing W_0 and its partial derivatives are approximated by numerical quadrature formulas.

In order to ensure that the numerical quadrature formulas are meaningful, there is an upper limit $p = P$ *and* $q = Q$ for the number of terms in the series for W_E [Eq. (11)]. The upper limits P and Q must satisfy the inequalities (see Ref. 4)

$$2P + 1 \leq M \tag{15a}$$

$$2Q + 1 \leq N \tag{15b}$$

where M and N are the number of rows and columns in the FEM data.

The integrations defined above result in a set of linear algebraic equations for a least-squares fit of the FEM nodal values of W and its derivative with respect to the outward normal on the plate boundary. These equations are solved for $(8P + 8Q)$ constants of integration and for the five undetermined coefficients in the polynomial W_{00}. Once the generalized coordinates are computed, the continuous function $W = W_E + W_I$ is used instead of the discrete function W_0 wherever W or its partial derivatives appear in the solutions of equations for U and V.

Continuous Solutions for U and V

The continuous solutions for U and V are computed by a method analogous to the method of solution for W. A double Fourier series is used to generate solutions U_I and V_I of the in-plane equilibrium equations (7a,b). Solutions of

$$L_{11}(U_E) + L_{12}(V_E) = 0 \tag{16a}$$

$$L_{12}(U_E) + L_{22}(V_E) = 0 \tag{16b}$$

are added so that continuous solutions of U and V are of the form

$$U = U_I + U_E \tag{17a}$$

$$V = V_I + V_E \tag{17b}$$

Constants of integration appearing in the solutions U_E and V_E are computed from a least-squares fit of FEM data for values of U and V at node points on the plate boundary.

The specific forms for U and V are

$$U_I = \sum_{m=0} \sum_{n=0} A_{1mn} \cos m\xi \cos n\eta + \sum_{m=1} \sum_{n=1} B_{1mn} \sin m\xi \sin n\eta + \sum_{m=0} \sum_{n=1} C_{1mn} \cos m\xi \sin n\eta + \sum_{m=1} \sum_{n=0} D_{1mn} \sin m\xi \cos n\eta \tag{18a}$$

$$V_I = \sum_{m=0} \sum_{n=0} A_{2mn} \cos m\xi \cos n\eta + \sum_{m=1} \sum_{n=1} B_{2mn} \sin m\xi \sin n\eta + \sum_{m=0} \sum_{n=1} C_{2mn} \cos m\xi \sin n\eta + \sum_{m=1} \sum_{n=0} D_{2mn} \sin m\xi \cos n\eta \tag{18b}$$

$$U_E = a_1 + b_1 x + c_1 y + \sum_{p=1} [F_{1p}(\eta)\cos p\xi + G_{1p}(\eta)\sin p\xi] + \sum_{q=1} [H_{1q}(\xi)\cos q\eta + I_{1q}(\xi)\sin q\eta] \tag{19a}$$

$$V_E = a_2 + b_2 x + c_2 y + \sum_{p=1} [F_{2p}(\eta)\sin p\xi + G_{2p}(\eta)\cos p\xi] + \sum_{q=1} [H_{2q}(\xi)\sin q\eta + I_{2q}(\xi)\cos q\eta] \tag{19b}$$

For solution of Eqs. (16), the functions $F_{1p}(\eta)$ and $F_{2p}(\eta)$ satisfy the pair of ordinary differential equations

$$A_{66}\beta^2 F''_{1p} - p^2 A_{11} F_{1p} + (A_{12} + A_{66})\beta p F'_{2p} = 0 \tag{20a}$$

$$-(A_{12} + A_{66})\beta p F'_{1p} + A_{22}\beta^2 F''_{2p} - p^2 A_{66} F_{2p} = 0 \tag{20b}$$

where primes denote differentiation with respect to η. The subscripted functions G, H, and I satisfy similar coupled ordinary differential equations. The complete solution of Eqs. (20) contains four constants of integration. The constants of integration are determined by boundary conditions on U and V.

$$U_E = U_0 - U_I \quad \text{for } x = 0 \tag{21a}$$

$$U_E = U_0 - U_I \quad \text{for } x = a \tag{21b}$$

$$V_E = V_0 - V_I \quad \text{for } x = 0 \tag{21c}$$

$$V_E = V_0 - V_I \quad \text{for } x = a \tag{21d}$$

$$U_E = U_0 - U_I \quad \text{for } y = 0 \tag{22a}$$

$$U_E = U_0 - U_I \quad \text{for } y = b \tag{22b}$$

$$V_E = V_0 - V_I \quad \text{for } y = 0 \tag{22c}$$

$$V_E = V_0 - V_I \quad \text{for } y = b \tag{22d}$$

The solution for the undetermined coefficients and constants of integration in U_E and V_E is similar to the solution for W_E. In particular, the number of terms in the series solutions must satisfy the inequalities in Eqs. (15). The polynomial coefficients a_1, b_1, c_1, a_2, b_2, and c_2 are determined by integrals similar in form to the integrals listed in the Appendix for the polynomial terms in W_E.

Residual Error

The least-squares solution for the generalized coordinates in U_E and V_E completes the analysis to determine a continuous solution for the plate displacements U, V, and W. The stress resultants N_x, N_y, N_{xy}, M_x, M_y, M_{xy}, Q_x, and Q_y are computed from the displacements and their derivatives. The output from the continuous solution can be computed at any given point or over a rectangular grid that is independent of the FEM grid.

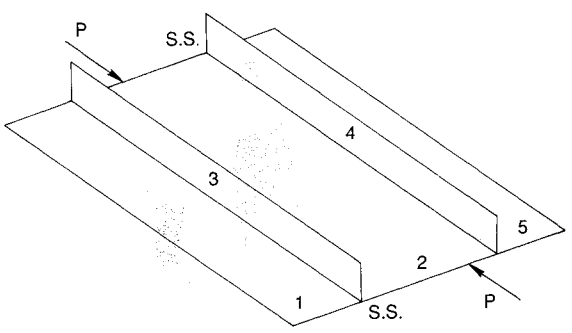

Fig. 1 Example of a plate component from a stiffened panel.

A measure of the error in the continuous solution derived from the FEM results is $E_3(x,y)$, the residual error in satisfying the transverse equilibrium equation (7c).

$$E_3 = L_{33}(W) - N_3(F, W + \bar{W}) \tag{23}$$

where W is now the continuous solution, and the in-plane stress resultants appearing in the bilinear operator are computed from the continuous solution.

The residual error has both theoretical and practical significance. In theory, the continuous solution for U, V, and W can be corrected by Newton's method.[1] An accurate correction requires an accurate computation for the residual error such as the result for E_3 computed in this paper. The residual error appears in the linear variational equations for the corrections on the displacements. The linear variational equations have variable coefficients and can be nearly singular for a postbuckled plate. Their solution requires additional numerical analysis and is not considered in the present paper.

However, from a practical point of view, rather than from a rigorous mathematical viewpoint, the residual error provides information on the accuracy of the continuous solution. Since the continuous solution is derived from the FEM solution, the residual error is also an indirect measure of the accuracy of the FEM results. This measure is not available in a finite-element solution based on direct minimization of a variational principle.

At points on the plate where the error is small, the FEM solution is probably good at the nodal points, and the continuous solution will be accurate for computing peak stresses that may occur near the nodes. Where the error is larger, it is probable that the percentage error in the displacements and the stress resultants are less than the comparable residual error, since the residual error contains higher-order partial derivatives than the stress resultants.

In general, the current computation of the error will not be small on the plate boundary. The error contains a "Gibb's

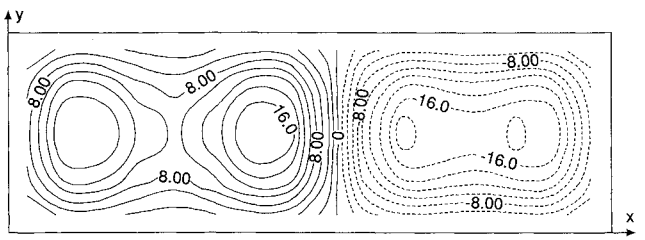

a) Discrete FEM solution

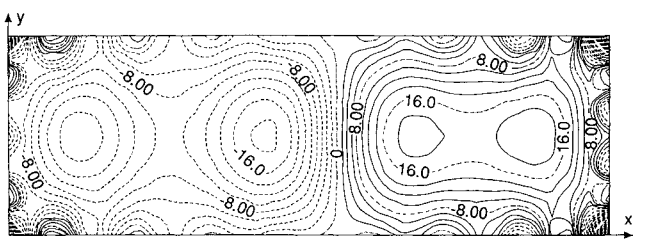

b) Continuous approximation[1]

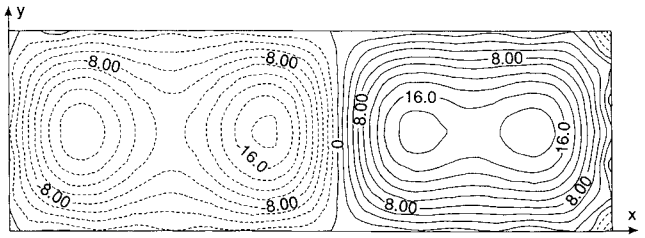

c) Continuous least-squares approximation

Fig. 2 Comparison of discrete and continuous moment resultant M_x.

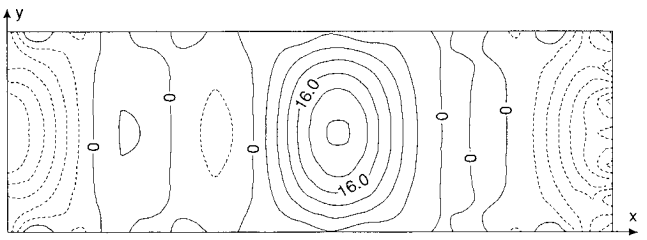

Fig. 3 Transverse shear Q_x.

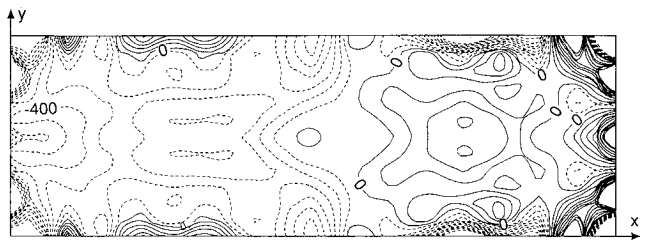

Fig. 4 Residual error in the transverse equilibrium equation $E_3/L_{33\max}$.

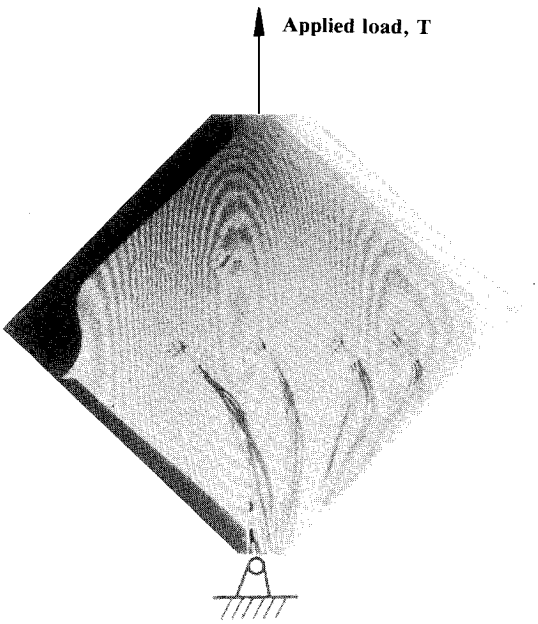

Fig. 6 Photograph of Moire-fringe pattern.

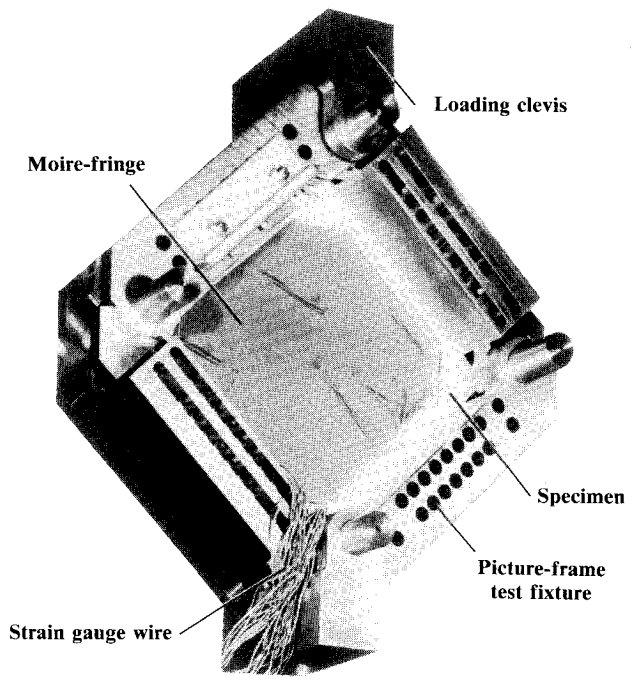

Fig. 5 Test specimen in picture-frame fixture.

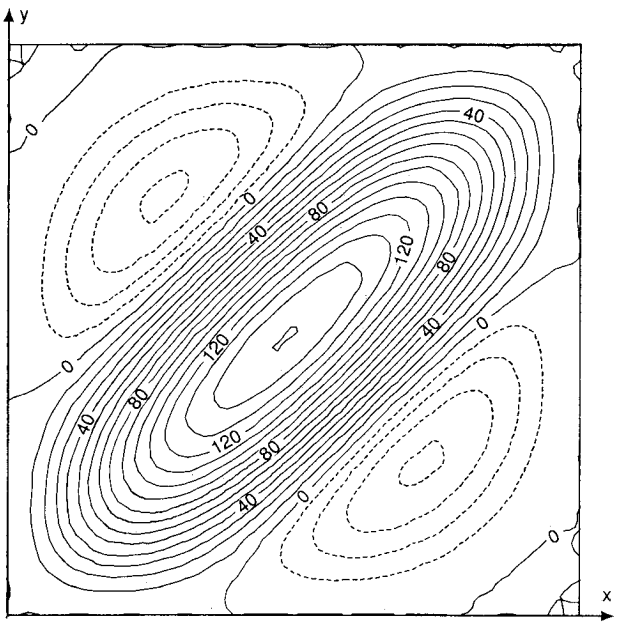

Fig. 7 Continuous transverse deflection W.

phenomenon'' near the boundary because of using a double sine series for W_I and for the imperfection $\bar{W}$. On the boundary

$$L_{33}(W_I) = 0$$

and

$$E_3 = N_3(F, W_E)$$

While away from the boundary, the general error is

$$E_3 = N_3(F_0, W_0 + \bar{W}) - N_3(F, W + \bar{W}) \tag{24}$$

from Eqs. (9).

Numerical Results and Error Analysis

The analysis to solve Eqs. (7) for a continuous displacement solution (U, V, W), derived from the discrete FEM results, has been programmed. Numerical results for two sample problems are presented below. The first example is the stiffened panel considered in Ref. 1. Results from the new analysis for the boundary conditions are compared to the corresponding results obtained from using the collocation method for the boundary conditions. The second example problem is a plate tested in shear, with measured initial imperfections.[3]

Comparison of Algorithms for Boundary Conditions

The least-squares method for boundary conditions was applied to the error analysis of FEM results for the blade-stiffened composite panel, loaded in compression into the postbuckling range, shown in Fig. 1. The panel was used as an example problem in Ref. 1 where the point matching method was used for the boundary conditions.

Typical results for a stress resultant in the central skin component are shown in Fig. 2 for the moment stress resultant M_x. The FEM results in Fig. 2a do not go all the way to the plate

boundaries. The FEM code tabulates stress resultants over a grid formed by the centroids of the rectangular elements. The contour plotting program does not extrapolate the discrete data and, consequently, the FEM data do not cover the complete plate. The closely spaced contours near the boundary in Fig. 2b are due to the oscillatory behavior of the continuous solution from Ref. 1 near the plate boundaries. In contrast, the continuous results from the current analysis using the least-squares method, shown in Fig. 2c, are much smoother.

Contour plots of the transverse shear resultant Q_x are shown in Fig. 3. The resultants Q_x and Q_y are not computed by the displacement model FEM code.

The residual error E_3 [Eq. (23)], normalized by dividing by the maximum computed absolute value of the linear operator L_{33}, is plotted in Fig. 4. The contour interval for the normalized error is 1%. The error is less than 5% of the maximum value of $L_{33}(W)$ in the region away from the boundaries. Close to the boundary the error is much higher because the solution contains a Gibb's phenomenon as previously discussed in the section on theory.

On the plate boundary, other measures of accuracy exist for the continuous solution. The two ends, $x = 0$ and $x = a$, are simply-supported. The bending moment resultant M_x should vanish on these edges. The continuous approximation matches the discrete FEM values of the rotation $W_{,x}$ on this boundary, and the residual M_x on the simply-supported edges is a measure of error, although it is not clear whether the error is in the continuous solution or in the edge rotations from the FEM solution. Continuous results for the plate element show that on the simply-supported edges, M_x varies from 0 to 8% of its maximum value (Fig. 2c).

Plate Tested in Shear

The present analysis takes into consideration the presence of initial imperfections in a plate. Numerical results are presented here for one of the panels tested by Rouse.[3] The plate analyzed

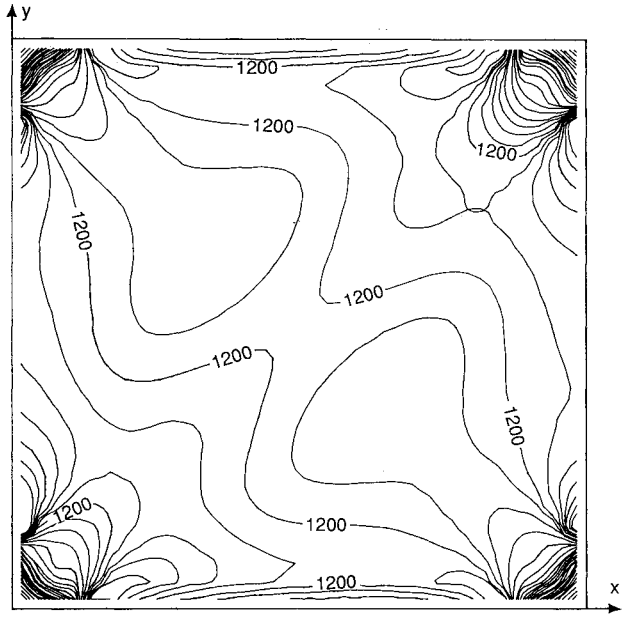

a) Discrete FEM solution

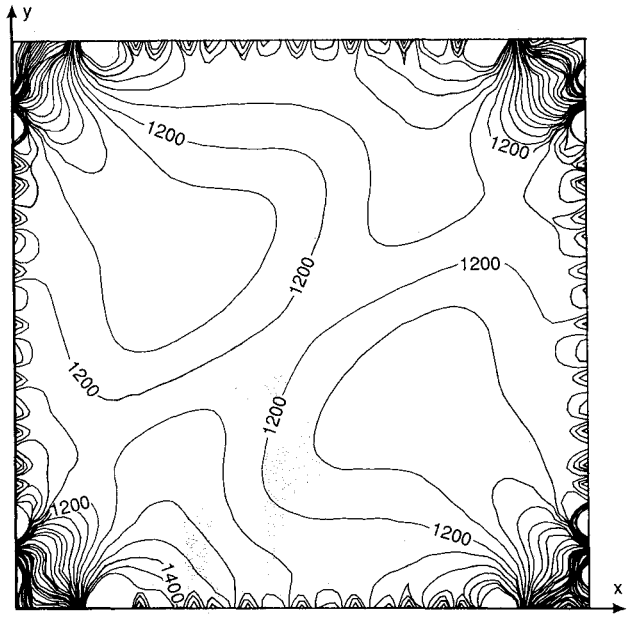

b) Continuous approximation

Fig. 8 Comparison of discrete and continuous stress resultant N_{xy}.

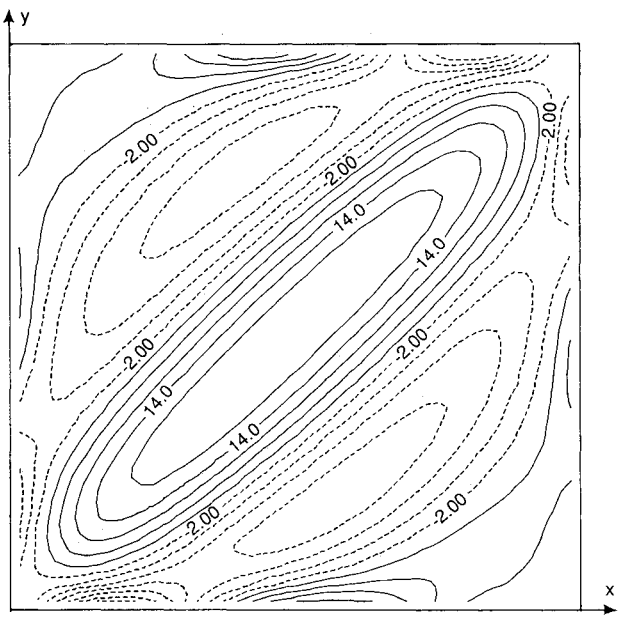

a) Discrete FEM solution

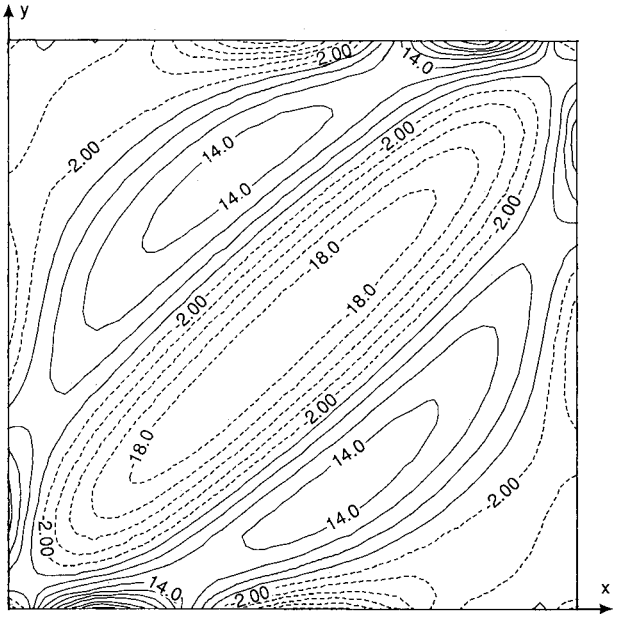

b) Continuous approximation

Fig. 9 Comparison of discrete and continuous moment resultant M_y.

Table 1 Data for sample problem

Property	Component	
	Skin	Stiffener
A_{11}, kips/in.	1262	871
A_{12}, kips/in.	379	261
A_{22}, kips/in.	937	647
A_{66}, kips/in.	381	263
D_{11}, in.-lb	742	244
D_{12}, in.-lb	223	733
D_{22}, in.-lb	551	181
D_{66}, in.-lb	224	738
Thickness, in.	0.084	0.058

Panel length, $a = 15.0$ in.
Middle plate width = 5.0 in.
Outer plate widths = 2.5 in.
Stiffener height = 1.4 in.
Load, $P = 15{,}792$ lb

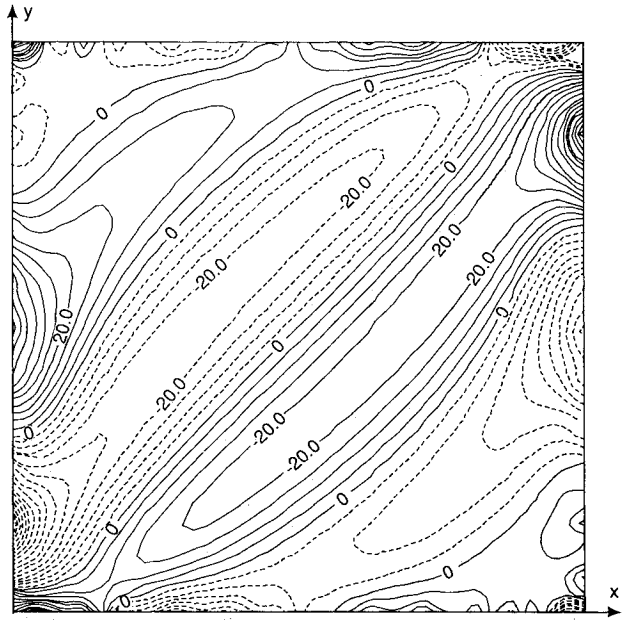

Fig. 10 Transverse shear Q_x.

here is a 16-ply graphite-epoxy laminate with a $[(\pm 45/0/90)_2]_S$ quasi-isotropic stacking sequence. A typical test specimen consisting of a plate attached to metal edge reinforcements and mounted in a picture-frame test fixture is shown in Fig. 5. Rouse[3] modeled the picture-frame fixture and the edge reinforcements as discrete beam elements. The plate was modeled by using a uniform grid of 32×32 quadrilateral plate elements. Surveys were conducted to measure the initial geometric imperfections of the plate. The shape of the initial imperfection is expressed as

$$\bar{W} = A \sin\frac{\pi x}{a} \sin\frac{\pi y}{b} \tag{25}$$

where the amplitude of the imperfection, $A = 0.0065$ in., is about 1-ply thickness. The FEM results for the example plate at a load twice the critical value are investigated herein.

A photograph of the moire-fringe pattern from a test is shown in Fig. 6, and can be compared to the contour plot of the continuous results for the out-of-plane displacement W shown in Fig. 7. The contour plots of the least-squares continous solution for the direct stress resultant N_{xy} and the bending moment stress resultant M_y are compared to the discrete FEM

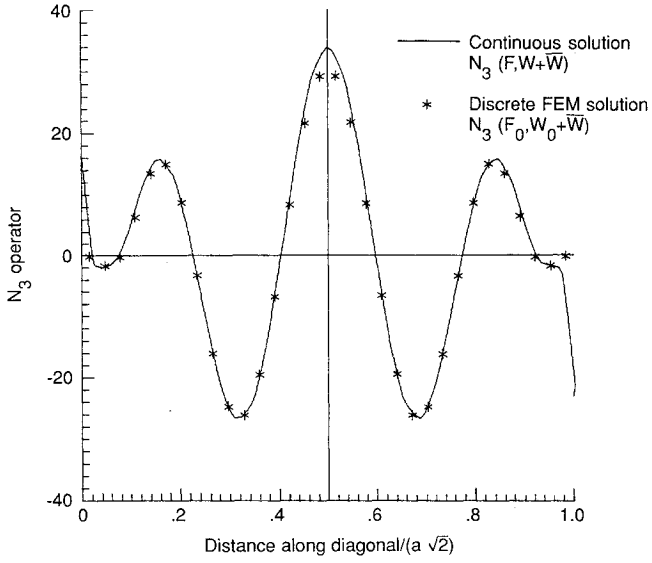

Fig. 11 Bilinear operators N_3 along diagonal $y = b - x$ of square plate tested in shear.

results in Figs. 8 and 9. Typical numerical results at selected points on the plate are listed in Table 1. The transverse shear stress resultant Q_x is shown in Fig. 10.

The residual error E_3 has dimensions of force-per-unit area and is the difference between the two operators N_3 for the FEM results and for the continuous results, equation (24). The two N_3 operators along the diagonal $y = b - x$ are plotted in Fig. 11.

Concluding Remarks

A general approach for determining a continuous solution in generalized coordinates from discrete finite-element results has been applied to plates. Numerical analysis is presented for computing the generalized coordinates for imperfect, rectangular, orthotropic postbuckled plates. The plates can be components of a general shell structure.

The numerical analysis has been programmed as a postprocessor for a general-purpose finite-element code. Numerical results for two example problems are presented in the paper. One plate is part of the skin for a stiffened panel in compression at twice the buckling load. The second plate is the test specimen in a picture-frame test fixture that simulates loading with pure shear deformations. In both examples, the finite-element solution for the given plate component is examined independently of the finite-element solution for the rest of the structure.

The continuous solution in generalized coordinates is computed as an approximate solution of the nonlinear plate equations. Furthermore, the solution satisfies displacement boundary conditions based on the finite-element displacements at nodal points on the plate boundary. Successive approximations prove to be a numerically stable method for computing continuous solutions of the plate equations. A least-squares solution for satisfying the nodal boundary conditions shows less oscillation between nodes than a collocation solution used in a previous paper. The oscillations in the earlier solution could have been due to minor details of convergence at end points of Fourier series rather than an intrinsic defect in the collocation method.

The residual error in the continuous solution in generalized coordinates is also computed for the two example problems. The residual error provides a measure of the error in the continuous solution as a solution of the nonlinear plate equations. Also, an accurate residual error, which is not computed by finite-element codes, is required if the continuous solution is to be further refined by Newton's method.

Appendix

This appendix contains details of the least-squares analysis of the boundary conditions. This analysis reduces the oscillatory behavior of the continuous solution between nodal points on the plate boundary compared to results using collocation. Two possible reasons for the improvement are less roundoff error and a different method for handling polynominal solutions.

Except for roundoff errors, the computation of the constants of integration in functions multiplied by trigonometric terms is the same for the two methods when the number of terms in the least-squares solution equals the number of terms in the collocation solution. For example, the constants of integration in the functions $W_{pc}(\eta)$, $W_{ps}(\eta)$, $W_{qc}(\xi)$, and $W_{qs}(\xi)$ that appear in W_E [Eq. (11)] are determined by similar sets of linear algebraic equations. The least-squares solution uses the orthogonality relations for the integrals of trigonometric functions explicitly, whereas the same orthogonality is implicit in the collocation method. In theory, the solution for two similar sets of algebraic equations should be identical; however, the possibility exists that the collocation solution was affected by roundoff errors.

It seems more likely that the changes in computation of the constants of integration in the polynomial solutions from that in Ref. 1 had more effect than reduced roundoff error. The polynomial solutions are W_{00} in Eq. (11) and the polynomial terms in the solutions U_E and V_E in Eqs. (19). In Ref. 1, the constants were computed by least-squares integrations over the plate surface. The constants are determined in the present numerical analysis by least-squares integrals on the boundary. The analysis for the constant a_{20} is an example. Because of the orthogonality of the trigonometric functions, the integral of $W_{E,x}$ on the side $x = 0$ reduces to

$$\int_0^b W_{E,x}(0,y)\mathrm{d}y = \int_0^b W_{00,x}(0,y)\mathrm{d}y + \frac{2\pi}{a}\Sigma p\int_0^b W_{ps}(\eta)\mathrm{d}y \tag{A1}$$

Integrating the same function on side $x = a$ reduces to

$$\int_0^b W_{E,x}(a,y)\mathrm{d}y = \int_0^b W_{00,x}(a,y)\mathrm{d}y + \frac{2\pi}{a}\Sigma p\int_0^b W_{ps}(\eta)\mathrm{d}y \tag{A2}$$

Subtracting Eq. (A1) from Eq. (A2) eliminates the sum of integrals of $W_{ps}(\eta)$

$$\int_0^b [W_{E,x}(a,y) - W_{E,x}(0,y)]\mathrm{d}y = \int_0^b [W_{00,x}(a,y) - W_{00,x}(0,y)]\mathrm{d}y \tag{A3}$$

Since

$$W_{00,x}(a,y) - W_{00,x}(0,y) = (a_{10} + 2a_{20}a) - a_{10}$$

the constant a_{20} is defined by

$$a_{20} = \frac{1}{2ab}\int_0^b [W_{E,x}(a,y) - W_{E,x}(0,y)]\mathrm{d}y \tag{A4}$$

In the numerical computations, the integral on the righthand-side is computed numerically using nodal values $W_{0,x}$ from the finite-element solution and the known values of $W_{I,x}$ [see Eqs. (13)]. Integrating on the sides $y = 0$ and $y = b$ gives a comparable result for the constant a_{02}:

$$a_{02} = \frac{1}{2ab}\int_0^a [W_{E,y}(x,b) - W_{E,y}(x,0)]\mathrm{d}x \tag{A5}$$

Similarly,

$$a_{10} = \frac{1}{ab}\int_0^b [W_E(a,y) - W_E(0,y)]\mathrm{d}y - aa_{20} \tag{A6}$$

$$a_{01} = \frac{1}{ab}\int_0^a [W_E(x,b) - W_E(x,0)]\mathrm{d}x - ba_{02} \tag{A7}$$

Finally, the constant a_{00}, a rigid-body displacement that does not appear in calculations for stress resultants, is computed by adding integrals. The result is

$$a_{00} = \frac{1}{2a}\left\{\int_0^a [W_E(x,0) - a_{10}x - a_{20}x^2]\mathrm{d}x - \frac{a}{2\pi}\Sigma\int_0^a W_{qc}(\xi)\mathrm{d}x\right\} + \frac{1}{2b}\left\{\int_0^b [W_E(0,y) - a_{01}y - a_{02}y^2]\mathrm{d}y - \frac{b}{2\pi}\Sigma\int_0^b W_{pc}(\eta)\mathrm{d}y\right\} \tag{A8}$$

The constants of integration on the right-hand side of Eq. (A7) are computed from equations that do not contain a_{00}. Therefore, a_{00} can be computed after computing the integrands in Eq. (A7) explicitly and using numerical integration.

References

[1]Thurston, G. A., Reissner, J. E., Stein, P. A., and Knight, N. F., Jr., "Error Analysis and Correction of Discrete Solutions from Finite-Element Codes," *AIAA Journal,* Vol. 26, April 1988, pp. 446–453.

[2]Thurston, G. A., Brogan, F. A., and Stehlin, P., "Postbuckling Analysis Using a General Purpose Code," *AIAA Journal,* Vol. 24, June 1986, pp. 1013–1020.

[3]Rouse, M., "Postbuckling of Flat Unstiffened Graphite-Epoxy Plates Loaded in Shear," *Proceedings of the AIAA/ASME/ASCE/AHS* 26th Structures, Structural Dynamics, and Materials Conference, Orlando, FL, April 15–17, 1985, AIAA, New York, pp. 605–616.

[4]Hildebrand, F. B., *Introduction To Numerical Methods*, McGraw-Hill, New York, 1956.